International Journal of Heat and Fluid Flow 30 (2009) 1080–1086

Contents lists available at ScienceDirect

International Journal of Heat and Fluid Flow

journal homepage: www.elsevier.com/locate/ijhff

Axisymmetric large eddy simulation of a circular source of buoyancy

Gérard C. Nihous *

University of Hawaii, Hawaii Natural Energy Institute, 1680 East-West Road, POST 109, Honolulu, HI 96822, USA

ARTICLE INFO

Article history:
Received 19 December 2008
Received in revised form 25 February 2009
Accepted 7 April 2009
Available online 9 May 2009

Keywords:
Axisymmetric numerical simulation
Turbulent mixing
Buoyancy

ABSTRACT

Axisymmetric large-eddy simulations (LES) of published experiments on vertical mixing above a circular source of buoyancy are performed. Numerical results confirm the existence of a mixing boundary layer just above the buoyancy source (freshwater injected into saline water). As experiments suggested, the calculated normalized shape of the boundary layer seems independent of source size, freshwater injection rate and background solute concentration. This validates a restrictive but numerically efficient assumption of axisymmetric turbulence for the LES calculations. It also lends additional credibility to the theoretical boundary-layer analysis of Epstein and Burelbach [Epstein, M., Burelbach, J.P., 2001. Vertical mixing above a steady circular source of buoyancy. Int. J. Heat Mass Trans. 44, 525–536], even at marginally high Froude numbers.

1. Theoretical background

Epstein and Burelbach (2001) developed a theoretical steady-state boundary-layer analysis describing the upward injection of a buoyant fluid at a velocity V_0 over a circular area of radius R_0 into another fluid of constant properties (subscript ∞). Their primary motivation was the assessment of flammability hazards (by analogy) when light fuel gas is released into quiescent air-filled storage containers. Their experimental setup consisted of a tank filled with brine and of a porous circular disk placed on the tank bottom through which freshwater could be injected. A schematic diagram of the physical problem under investigation is shown in Fig. 1. It should be noted that such a configuration could be useful in describing diffuse hydrothermal vents on the ocean floor as well (Lupton et al., 1985; Bemis et al., 2002). Both data and theory successfully showed the existence of a mixing boundary layer above the buoyancy source as ambient fluid is drawn radially inward until conditions for the existence of a rising plume are met, at a transition radius $r = R_p$. Perhaps the most compelling results were that the shape of the boundary layer as well as the transition radius normalized with R_0 appear to be independent of source size (R_0), freshwater injection rate (V_0) and background solute concentration (Y_∞).

Model assumptions are not all discussed here unless they are of special relevance, and additional details can be found in Epstein and Burelbach (2001). Following Baird and Rice (1975), the vertical dispersion coefficient E was assumed to be of the form $l^2[(g/\rho)\,\partial\rho/\partial z]^{0.5}$ where g is the gravitational acceleration, z the vertical coordinate and ρ the local fluid density; the characteristic length scale l was further expressed as $\beta\delta\,(r)$, i.e. proportional to the boundary-layer thickness δ given the wide radial extent of the fluid domain (Epstein and Burelbach, 2000). The Boussinesq approximation whereby fluid density is constant except in the body-force term of the vertical momentum equation was adopted and density was linearly approximated as a function of salt mass fraction Y, i.e. $\rho \approx \rho_0\,(1 + kY)$. A simplification of the boundary condition expressing that no salt is passing through the porous disk was made provided that the densimetric Froude number $F = V_0\{gR_0\,(\rho_\infty - \rho_0)/\rho_\infty\}^{-1/2}$ is small.[1] Yet, we found that it was possible to complete the boundary-layer analysis with the full boundary condition below, instead of Eq. (14) in Epstein and Burelbach (2001):

$$V_0 Y_\infty = 3V_0(Y_\infty - \overline{Y}) + 6^{3/2}\beta^2(gk)^{1/2}\delta^{1/2}(Y_\infty - \overline{Y})^{3/2} \tag{1}$$

Omitting details, the following results for the boundary-layer thickness δ and average salt mass fraction in the mixing layer $\overline{Y}$ were obtained instead of Eqs. (20) and (22) in Epstein and Burelbach (2001):

$$\delta = R_0\left[3F^{2/3}\left(\frac{1-\eta^2}{\eta}\right)^{2/3} + 6^{3/2}\beta^2\left(\frac{1-\eta^2}{\eta}\right)\right] \tag{2}$$

$$Y_\infty - \overline{Y} = \frac{Y_\infty}{3 + \frac{6^{3/2}\beta^2}{F^{2/3}}\left(\frac{1-\eta^2}{\eta}\right)^{1/3}} \tag{3}$$

It can be verified that in the limit $F \to 0$, the published results are recovered, except that the apparent singularity for $\overline{Y}$ at $r = R_0$ ($\eta = 1$) is now lifted and replaced with the anticipated finite value $2Y_\infty/3$ corresponding to $Y(R_0, 0) = 0$ (freshwater).

* Tel.: +1 808 956 2338; fax: +1 808 956 2336.
E-mail address: nihous@hawaii.edu

[1] This definition of F is $\sqrt{2}$ times that in Epstein and Burelbach (2001), for simpler solution coefficients

0142-727X/$ - see front matter © 2009 Elsevier Inc. All rights reserved.
doi:10.1016/j.ijheatfluidflow.2009.04.002

Nomenclature

C_K	Kolmogorov constant
C_{SM}	Smagorinsky constant (0.1)
D	turbulent diffusivity ($m^2\ s^{-1}$)
E	dispersion coefficient for vertical mixing ($m^2\ s^{-1}$)
E_0	entrainment coefficient for plume (0.12)
F	densimetric Froude number; $V_0\{gR_0(\rho_\infty - \rho_0)/\rho_\infty\}^{-1/2}$
g	gravitational acceleration ($m\ s^{-2}$)
h	finite-element grid size (m)
k	constant of proportionality between water density and salt concentration (0.64)
l	characteristic mixing length for turbulent diffusion (m)
P	pressure (Pa)
Q	inward volume flux within mixing layer ($m^3\ s^{-1}$); $2\pi r\delta\bar{u}$
Q_p	volume flux from mixing layer into rising plume ($m^3\ s^{-1}$)
r	radial coordinate (m)
R_0	radius of source of buoyant fluid (m)
$\vec{u}$	velocity vector ($m\ s^{-1}$)
$\bar{u}$	average radial inward velocity in mixing boundary layer ($m\ s^{-1}$)
V_0	upward velocity of injected fluid (m)
Y	salt mass fraction
Y_p	average salt mass fraction at plume neck
$\overline{Y}$	average salt mass fraction in mixing boundary layer
z	vertical coordinate (m)

Greek letters

α	molecular salt diffusivity ($m^2\ s^{-1}$)
β	mixing-length thickness proportionality coefficient (0.14)
δ	vertical thickness of mixing boundary layer (m)
η	non-dimensional radial coordinate
μ	dynamic viscosity ($kg\ m^{-1}\ s^{-1}$)
μ_0	molecular dynamic viscosity ($kg\ m^{-1}\ s^{-1}$)
ν	kinematic viscosity ($m^2\ s^{-1}$); $\nu_0 + \nu_{SM}$
ν_0	molecular kinematic viscosity ($m^2\ s^{-1}$)
ν_{SM}	turbulent kinematic viscosity ($m^2\ s^{-1}$)
ρ	water density ($kg\ m^{-3}$)
ρ_0	freshwater density ($kg\ m^{-3}$)

Subscripts

p	properties at transition from mixing boundary layer to buoyant plume
r	radial direction
z	vertical direction
θ	tangential direction
∞	ambient water

Next the approximate volume and salt balances at the transition radius R_p between mixing layer and rising plume, Eq. (25) in Epstein and Burelbach (2001), were replaced by exact though straightforward expressions. For the overall volume flux Q_p from the mixing layer into the rising plume, we have $Q_p = Q(R_p) + \pi R_p^2 V_0$. For the average salt mass fraction Y_p at the rising plume neck, $Y_p = Q(R_p)\overline{Y}(R_p)/Q_p$. Using those relationships into Eq. (43) in Epstein and Burelbach (2001) results in an implicit equation for η_p:

$$4E_0F^2\left[(1-\eta^2)\left\{3+\frac{6^{3/2}\beta^2}{F^{2/3}}\left(\frac{1-\eta^2}{\eta}\right)^{1/3}\right\}+\eta^2\right]^3=\eta^5 \qquad (4)$$

In the low-Froude-number limit, Eq. (4) becomes $4\ 6^{9/2}E_0\beta^6(1\text{-}\eta^2)^4 = \eta^6$. Epstein and Burelbach (2001) obtain the same equation with $(1-\eta^2)$ raised to an exponent 3, which makes the equation solvable explicitly; with β and E_0 about 0.14 and 0.12, respectively, the solution is quite insensitive to the exponent of $(1-\eta^2)$: η_p would be over-predicted by only 3%. Eq. (4) also suggests that a mixing boundary layer would not form if the Froude number exceeds $(4E_0)^{-1/2} \approx 1.44$ for which $\eta_p = 1$.

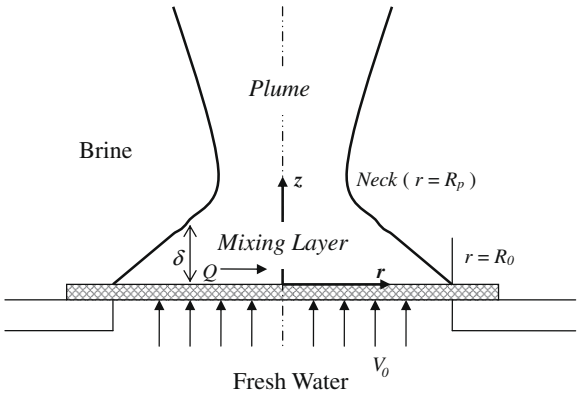

Fig. 1. Schematic diagram and selected notation for the experimental setup of Epstein and Burelbach (2001); remote tank boundaries are not shown.

At this juncture, a puzzling question arises given that the Froude numbers for the experiments are not small enough for Eq. (2) to match the experimental data (cf. Table 1); the range for F is also too wide to simply redefine the constant β estimated by Epstein and Burelbach (2001) to be 0.14. In other words, a relaxation of one model assumption (i.e. a more exact boundary condition) has led to a mismatch between theory and experiment. There is no obvious explanation why the low-Froude-number limit apparently performs better than a more complete solution at moderate values of F. Although large reported experimental uncertainties (±20%) in identifying the boundary layer must be kept in mind, it is also possible that discarding the convective term $3V_0(Y_\infty - \overline{Y})$ in Eq. (1) actually compensates for the effects of other assumptions and approximations on model accuracy.

2. Axisymmetric large eddy simulation

To further investigate the results presented in Epstein and Burelbach (2001), numerical simulations of their experiments were undertaken. The approach adopted here is to use sufficiently fine finite-element grids to resolve the buoyancy-driven production of kinetic energy (and the associated 'large' eddies). Turbulence then can be represented by the relatively simple Smagorinsky model based on a balance between shear-driven production and dissipation of subgrid-scale kinetic energy. Large eddy simulation (LES) has become a widespread method for numerical investigations of turbulent fluid flows, especially since computers have become more powerful (Lesieur and Metais, 1996; Alendal and Drange, 2001; Pesteanu and Schwerdtfeger, 2003; Felten et al., 2004).

To make calculations practical on a single-processor computer, the fluid domain under consideration and the velocity and salt concentration fields were assumed to be axisymmetric about the vertical axis through the center of the buoyancy source. Accordingly, the tangential velocity u_θ and partial derivatives $\partial/\partial\theta$ are identically set to zero henceforth. This choice is consistent with the circular geometry of the buoyancy source, but not with the rectangular footprint of the tank used in the experiments. The overall

Table 1
Experimental and simulation parameters.

Experiment #	1	2	3	4	5	6
R_0 (m)	0.0572	0.0572	0.114	0.114	0.114	0.178
V_0 (m s^{-1})	0.0200	0.0270	0.0021	0.0054	0.0084	0.0066
Y_∞	0.087	0.141	0.169	0.146	0.122	0.136
F	0.113	0.120	0.006	0.017	0.028	0.017
Y at transition (± 0.001)	0.083	0.135	0.162	0.140	0.117	0.130
Simulation time (s)	10	7	12	12	11	16
Snapshot range in Fig. 2 (every second)	5–10	6–7	9–12	6–12	5–11	8–13

horizontal area of the tank (0.66 m^2), however, was deemed large enough ($\gg \pi R_0^2$) to preclude side-wall effects so that the precise shape of the outer boundaries should not be important. The assumption of axisymmetric flow and concentrations seems reasonable, in an average sense at least, for this particular problem, but it can be questioned in principle since turbulence is inherently asymmetric at a given time. Axisymmetric problems have been considered before as computationally efficient shortcuts for full three-dimensional configurations (Mahalingam et al., 1990; Mell et al., 1996). More recently, axisymmetric turbulence alone has been used in otherwise three-dimensional formulations (Jacques et al., 2002; Randriamampianina et al., 2004); detailed discussions of the validity of the axisymmetry assumption are provided in these latter references.

Within the axisymmetric fluid domain of radius 0.45 m and height 0.75 m closely representative of the experimental tank, the following coupled partial differential equations are solved:

$$\nabla \cdot \vec{u} = 0 \tag{5}$$

$$\rho \frac{\partial \vec{u}}{\partial t} + \rho(\vec{u} \cdot \nabla)\vec{u} = \nabla \cdot (-P[I] + \mu[\nabla \vec{u} + (\nabla \vec{u})^T]) + \vec{F} \tag{6}$$

$$\frac{\partial Y}{\partial t} + \vec{u} \cdot \nabla Y = \nabla \cdot (D \nabla Y) \tag{7}$$

The first two are the incompressible Navier–Stokes equations, and the third the advection–diffusion equation for salt. $[I]$ is the identity tensor and ∇ the Nabla operator. The fluid velocity vector $\vec{u}$ has two components u_r and u_z in the radial and vertical directions. To further simplify the analysis, water density ρ is taken as a constant ($\rho_0 = 1000$ kg/m^3) except in the body force $\vec{F}$ (Boussinesq approximation); $\vec{F}$ has no radial component, but its vertical component is equal to $\rho_0 g(Y_\infty - Y)$. In this simplified formulation, hydrostatic pressure and background weight cancel out so that P is interpreted as the remaining dynamic pressure. μ is the dynamic viscosity and is the sum of a molecular term and of a turbulent (subgrid) expression discussed further below; this formalism is representative of first-order turbulence closure schemes where Reynolds stresses are parameterized.

Initial conditions at $t = 0$ are $\vec{u} = \vec{0}$, $P = 0$ and $Y = Y_\infty$. Boundary conditions for the Navier–Stokes equations are $\vec{u} = \vec{0}$ along the outer wall and on the bottom for $r > R_0$ (no slip) and $\vec{u} = (0, V_0)$ on the bottom for $r \leqslant R_0$ (water injection); the upper free surface is simplified as a rigid lid subject to the slip condition $u_z = 0$, and outflow is allowed to occur at $P = 0$ along the upper 5 cm of the outer vertical wall. All boundaries are insulated as far as salt transfer is concerned, except for the small outflow segment where a convective flux (zero gradient) is enforced.

The kinematic viscosity $\nu = \mu/\rho \approx \mu/\rho_0$ is the sum of a molecular term $\nu_0 = \mu_0/\rho_0$, of the order of 10^{-6} m^2 s^{-1}, and of a turbulent term ν_{SM} defined as follows for this axisymmetric problem:

$$\nu_{SM} = (c_{SM} h)^2 \sqrt{2\left[\left(\frac{\partial u_r}{\partial r}\right)^2 + \left(\frac{\partial u_z}{\partial z}\right)^2 + \left(\frac{u_r}{r}\right)^2\right] + \left(\frac{\partial u_r}{\partial z} + \frac{\partial u_z}{\partial r}\right)^2} \tag{8}$$

h is interpreted as an average finite-element mesh size, and c_{SM} is the Smagorinsky constant which can be related to the Kolmogorov constant c_K as $(3c_K/2)^{-3/4}/\pi$ (Lesieur and Metais, 1996). c_{SM} is selected here as 0.1; this value is consistent with choices in the technical literature (Lesieur and Metais, 1996; Alendal and Drange, 2001; Pesteanu and Schwerdtfeger, 2003) and corresponds to a Kolmogorov constant when anisotropy and acceleration fluctuations significantly contribute to the energy budget (Heinz, 2002). Following a parameterization based on renormalization group theory, the overall diffusivity D can then be obtained by solving an implicit equation for the ratio D/ν (Yakhot and Orszag, 1986). A close explicit approximation was derived instead to avoid the numerical burden of an implicit equation:

$$D = \nu\left[1.3929 - \left(1.3929 - \frac{\alpha}{\nu_0}\right)\left(\frac{\nu_0}{\nu}\right)^{1.78}\right] \tag{9}$$

Without turbulence, $\nu = \nu_0$ and D would be equal to the molecular diffusivity α (about 1.5×10^{-9} m^2 s^{-1} for salt); in very turbulent areas ($\nu \gg \nu_0$), $D \approx 1.3929\,\nu$.

The six physical experiments conducted by Epstein and Burelbach (2001) were numerically simulated. A commercial finite-element package (FEMLAB® 3, Version 3.1, 2003) was used to solve Eqs. (5)–(9) subject to the initial and boundary conditions discussed earlier. No artificial diffusion was added and the software's general solution form rather than the weak form was selected. The formulation of Eq. (6) with the total stress tensor inside the divergence operator allows shear-rate dependent viscosity (as in the modeling of non-Newtonian fluids). Default settings and options were adopted as much as possible, including the direct linear solver UMFPACK (based on the unsymmetric-pattern multifrontal method and direct LU factorization). The parameters R_0, V_0 and Y_∞ defining each experiment are listed in Table 1. Numerical grids of about 25 000 elements corresponding to an average mesh size h of the order of 5.7 mm were used; element quality was higher than 0.5. Results obtained at such spatial resolution were found to be insensitive to further grid refinement; this issue is discussed in more details at the end of the section. Simulation times varied between 7 and 16 s depending on the convergence rate (cf. Table 1); this corresponded to computer runtimes of several hours (1.86 GHz processor with 2 GB RAM). In all cases, turbulent viscosity was activated after a simulation time of 0.1 s. A quasi steady-state for the mixing boundary layer seemed to be reached rapidly (t of the order of 4–6 s); because of highly turbulent conditions, this was estimated visually from 1-s solution snapshots of the salt mass fraction. Fig. 2 shows sample calculated values of the salt mass fraction for Experiment # 6 at $t = 12$ s, with arrows representing the velocity field.

For each set of numerical simulations, points where Y was within 0.001 of a salinity threshold approximately equal to 0.96 Y_∞ (cf. Table 1) were used to track the edge of the mixing boundary layer at low vertical coordinates. Fig. 3 shows 32 snapshots of those 'boundary points' from all simulations (every second in the time intervals listed in Table 1). Time intervals for the data in Fig. 3 were selected without the first few seconds (transient phase), and in the case of Experiment # 6, without the period between 13 and 16 s

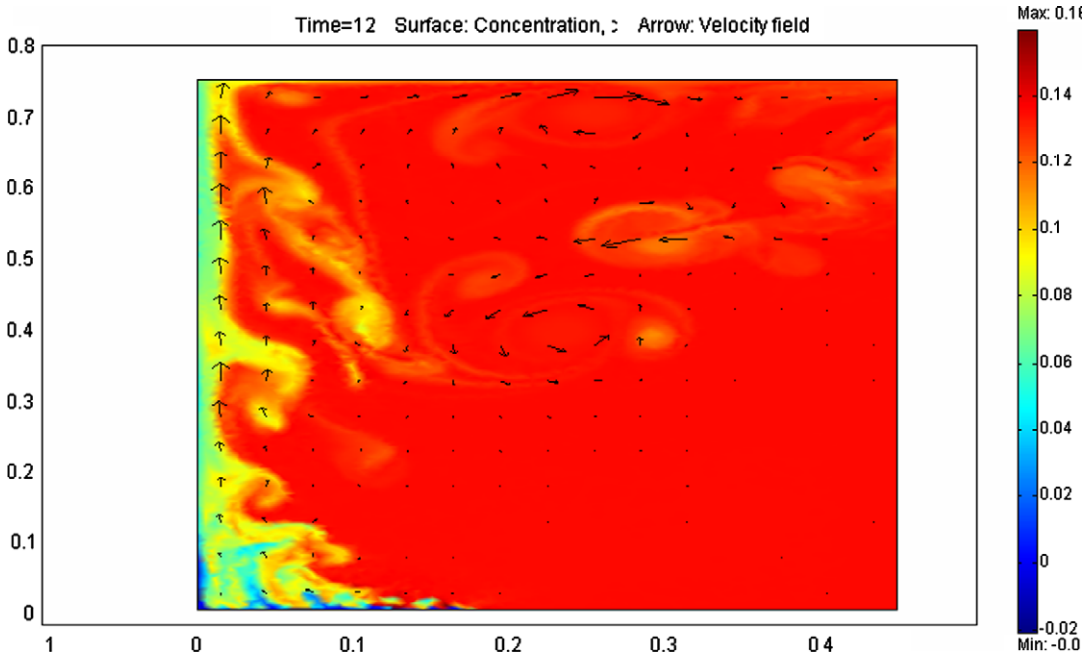

Fig. 2. Snapshot of LES calculations of salt mass fraction for Experiment # 6 at $t = 12$ s (axis dimensions in meters).

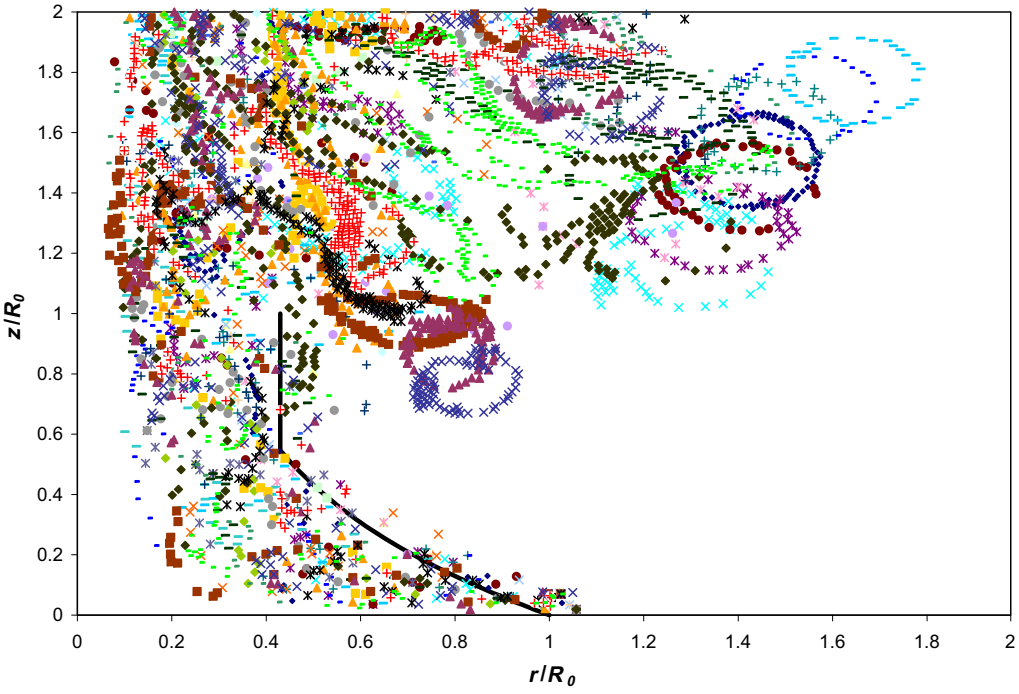

Fig. 3. Selected snapshots of calculated salt-mass-fraction transitions for all simulated experiments (cf. Table 1).

where eddies detached from the rising plume somewhat obscured the edge of the mixing boundary layer below. Also shown as thick lines (as well as in Figs. 4 through 7) are the fundamental results from Epstein and Burelbach (2001): the normalized boundary-layer thickness from Eq. (2) with $F = 0$ and $\beta = 0.14$; and a vertical line (of arbitrary height) marking the plume transition at $R_p = 0.43\ R_0$. Given the highly turbulent nature of the flows and the absence of any time averaging in constructing Fig. 3, the agreement between numerical simulations and the low-Froude-number analysis is remarkable.

Fig. 4 shows the boundary points for Experiment # 6 from 6 to 16 s. The inclusion of the time intervals from 6 to 8 s and from 13 to 16 s that were not used in Fig. 3 smears the edge of the mixing layer and of the plume transition. The complete solution for Y (Experiment # 6) was then time averaged between 6 and 16 s. Fig. 5 is a plot of the time-averaged values of the salt mass fraction when they fall below 0.130. Time averaging has strongly smoothed the highly irregular solution and brought the numerical simulations in close agreement with both the data (not shown) and the low-Froude-number analysis of Epstein and Burelbach (2001).

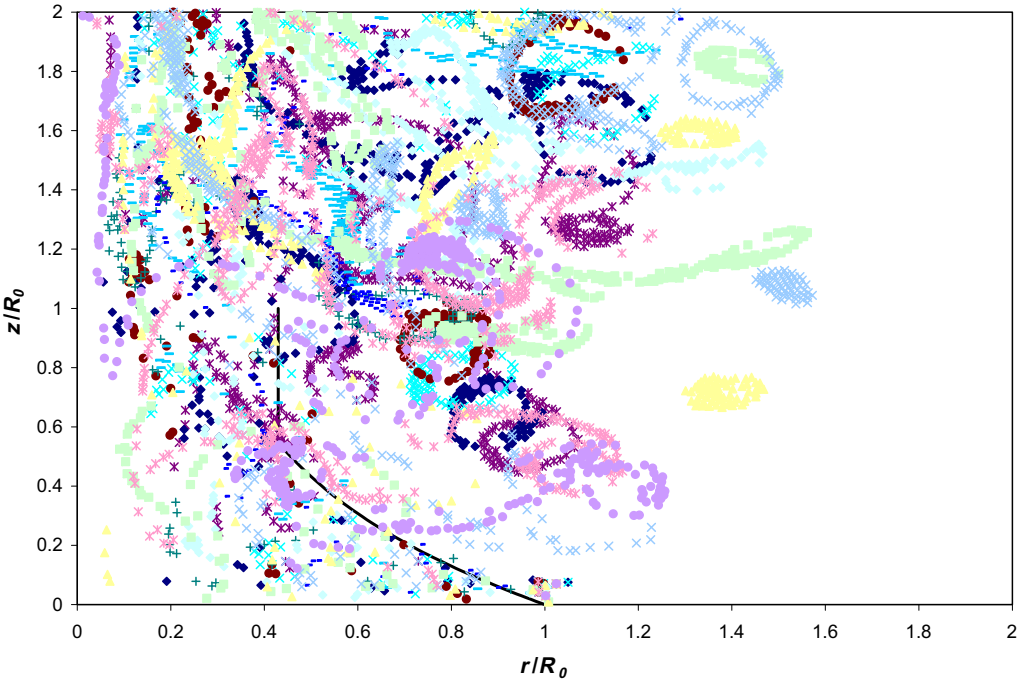

Fig. 4. Snapshots of calculated salt-mass-fraction transition for Experiment # 6: $Y = 0.130 \pm 0.001$ every second from 6 s to 16 s.

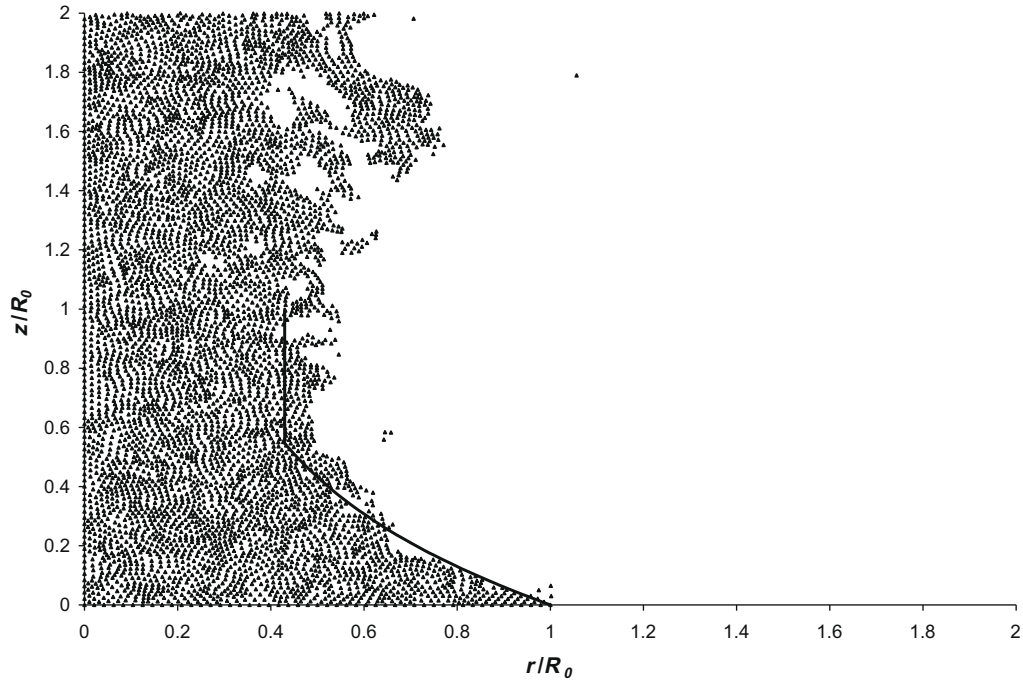

Fig. 5. Time averages (from 6 s to 16 s) of calculated salt mass fractions for Experiment # 6: values below 0.130.

Finally, the effect of grid refinement is considered. Fig. 6 (corresponding to Experiment # 3) demonstrates that an average mesh size <*h*> as large as 11.4 mm, or twice the baseline value, essentially reproduces the mixing-layer boundary within the same simulation time frame. A choice of coarser grids may violate the implicit assumptions of Smagorinsky-type closures, e.g. if buoyancy becomes significant in the production and transport of turbulent kinetic energy at subgrid scales. With <*h*> = 30 mm, for example, the complex flow structure displayed in Figs. 2–4 is not resolved. In this case, Fig. 7 shows that a mixing-layer boundary is not predicted to develop within about 10 s. When these coarse simulations are run over substantially greater times, however, a stable mixing-layer boundary appears. Hence, such a boundary seems to be a robust feature of the problem under consideration.

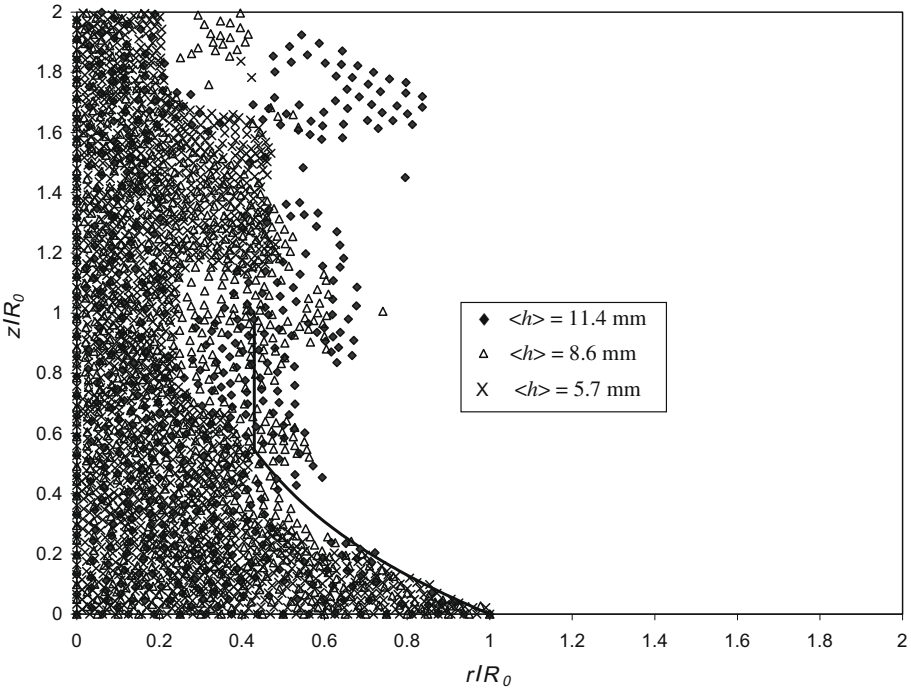

Fig. 6. Time averages (from 9 s to 12 s) of salt mass fractions (< 0.162) for Experiment # 3 with different average mesh size <*h*>.

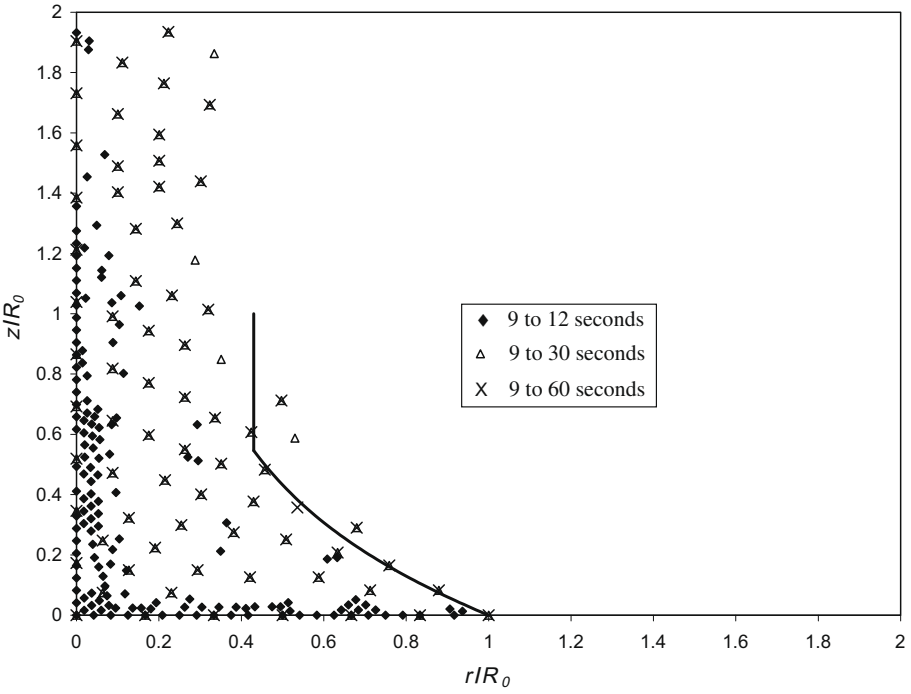

Fig. 7. Different time averages of salt mass fractions (<0.162) for Experiment # 3 with coarse average mesh size (<*h*> = 30 mm).

3. Conclusions

This study presented a critical evaluation of a published theoretical and experimental investigation of vertical mixing above a circular source of buoyancy. Normalized data showing the existence of a mixing boundary layer that is independent of several experimental parameters could be reproduced well with axisymmetric large-eddy numerical simulations. This lent additional credibility to the theoretical boundary-layer analysis of Epstein and Burelbach (2001), even though relaxing some of their model's assumptions failed to preserve a good agreement between theory and experiments given the range of Froude numbers under consideration.

Acknowledgement

Funding for this study was provided by the Office of Naval Research through the Hawaii Energy and Environmental Technology Initiative.

References

Alendal, G., Drange, H., 2001. Two-phase, near-field modeling of purposefully released CO_2 in the ocean. J. Geophys. Res. 106, 1085–1096.

Baird, M.H.I., Rice, R.G., 1975. Axial dispersion in large unbaffled columns. Chem. Eng. J. 9, 171–174.

Bemis, K.G., Rona, P.A., Jackson, D., Jones, C., Silver, D., Mitsuzawa, K., 2002. A comparison of black smoker hydrothermal plume behavior at Monolith Vent and at Clam Acres Vent Field: dependence on source configuration. Marine Geophys. Res. 23, 81–96.

Epstein, M., Burelbach, J.P., 2000. Transient vertical mixing by natural convection in a wide layer. Int. J. Heat Mass Transfer 43, 321–325.

Epstein, M., Burelbach, J.P., 2001. Vertical mixing above a steady circular source of buoyancy. Int. J. Heat Mass Transfer 44, 525–536.

Felten, F., Fautrelle, Y., Du Terrail, Y., Metais, O., 2004. Numerical modeling of electromagnetically-driven turbulent flows using LES methods. Appl. Math. Model 28, 15–27.

FEMLAB, 2003. Multiphysics Modeling, Version 3.1, COMSOL Inc.

Heinz, S., 2002. On the Kolmogorov constant in stochastic turbulence models. Phys. Fluids 14, 4095–4098.

Jacques, R., Le Quéré, P., Daube, O., 2002. Axisymmetric numerical simulations of turbulent flows in rotor–stator enclosures. Int. J. Heat Fluid Flow 23, 381–397.

Lesieur, M., Metais, O., 1996. New trends in large-eddy simulations of turbulence. Annu. Rev. Fluid Mech. 28, 45–82.

Lupton, J.E., Delaney, J.R., Johnson, H.P., Tivey, M.K., 1985. Entrainment and vertical transport of deep-ocean water by buoyant hydrothermal plumes. Nature 316, 621–623.

Mahalingam, S., Cantwell, B.J., Ferziger, J.H., 1990. Full numerical simulation of coflowing, axisymmetric jet diffusion flames. Phys. Fluids A 2, 720–728.

Mell, W.E., McGrattan, K.B., Baum, H.R., 1996. Numerical simulation of combustion in fire plumes. In: Proc. 26th Int. Symp. Comb., pp. 1523–1530.

Peşteanu, O., Schwerdtfeger, K., 2003. Contribution to the large eddy simulation of flows in electromagnetic stirrers for continuous casting. ISIJ Int. 43, 1556–1561.

Randriamampianina, A., Schiestel, R., Wilson, M., 2004. The turbulent flow in an enclosed corotating disk pair: axisymmetric numerical simulation and Reynolds stress modeling. Int. J. Heat Fluid Flow 25, 897–914.

Yakhot, V., Orszag, S.A., 1986. Renormalization group analysis of turbulence, I: basic theory. J. Sci. Comput. 1, 3–51.